A longitudinal Health Atlas of age-associated multisystem physiology from population health examinations in China

Shilong Zhang[1], Qing Yang[2], Huiyun Pan[3], Enyan Liu[1], Yifan Chen[1], Qiuyu Fang[1], Luyao Xie[1], Zixuan Wang[1], Zhimeng Zhao[1], Cong Feng[1, 4, 5, *], Ming Chen[1, 4, 5, *]

[1] Department of Bioinformatics, College of Life Sciences, Zhejiang University, Hangzhou 310058, P.R. China.

[2] Zhejiang Provincial Center for Disease Control and Prevention, Hangzhou 310051, P.R. China.

[3] Department of Geriatrics, The First Affiliated Hospital of Zhejiang University, Hangzhou 310003, P.R. China.

[4] State Key Laboratory of Vegetation Structure, Function and Construction, College of Life Sciences, Zhejiang University, Hangzhou 310058, P.R. China.

[5] Zhejiang Key Laboratory of Multi-omics Precision Diagnosis and Treatment of Liver Diseases, Department of General Surgery, Sir Run-Run Shaw Hospital, Zhejiang University School of Medicine, Hangzhou 310016, P.R. China.

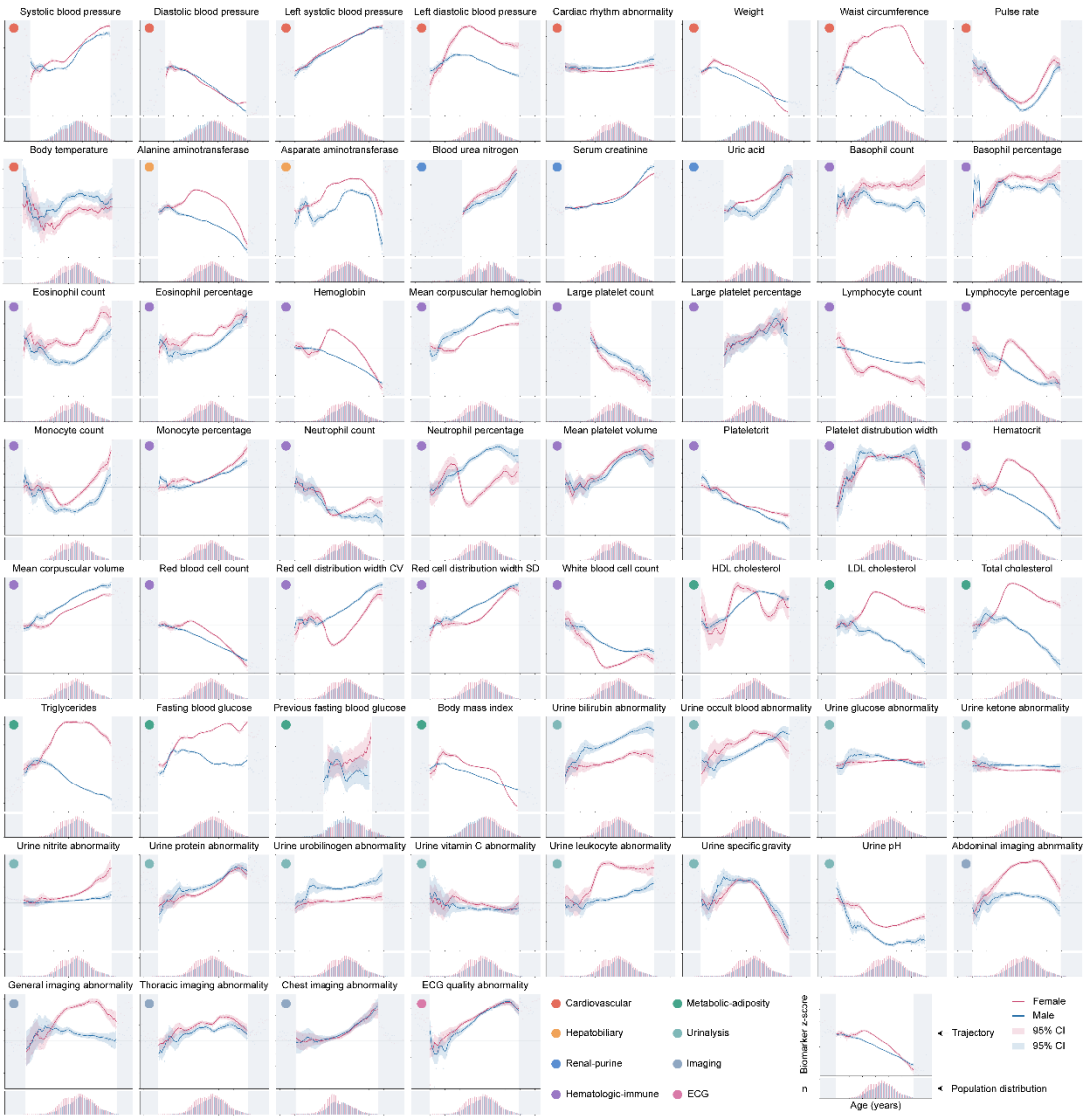
* Corresponding Authors: Ming Chen, Cong Feng

Email: mchen@zju.edu.cn, ventson@zju.edu.cn

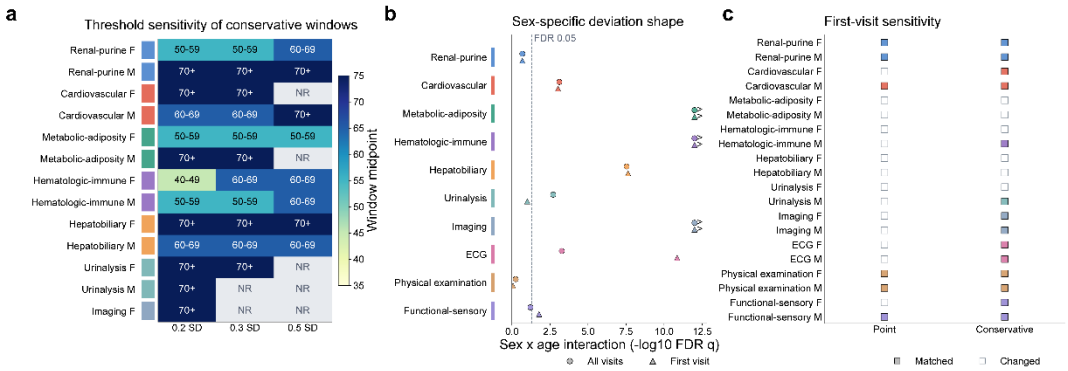
Supplementary information

SI Figures		
SI 1	**Supplementary Fig. 1 |** Sex-specific age trajectories across the Health Atlas biomarker panel	P4
SI 2	**Supplementary Fig. 2 |** Sensitivity analyses for detectable clinical phenotype shift windows	P5
SI 3	**Supplementary Fig. 3 |** Robustness of atlas-state mortality associations.	P6
SI 4	**Supplementary Fig. 4 |** Summary properties of the age-banded module co-deviation network	P7
SI 5	**Supplementary Fig. 5 |** Biomarker-level co-deviation structure in participants aged 30–39 years	P8
SI 6	**Supplementary Fig. 6 |** Biomarker-level co-deviation structure in participants aged 40–49 years	P9
SI 7	**Supplementary Fig. 7 |** Biomarker-level co-deviation structure in participants aged 50–59 years	P10
SI 8	**Supplementary Fig. 8 |** Biomarker-level co-deviation structure in participants aged 60–69 years	P11
SI 9	**Supplementary Fig. 9 |** Biomarker-level co-deviation structure in participants aged 70 years and older	P12
SI 10	**Supplementary Fig. 10 |** Multi-omics anchoring of atlas-derived aging axes	P13
SI 11	**Supplementary Fig. 11 |** Partial external transport and temporal validation of the Health Atlas framework.	P14
SI 12	**Supplementary Fig. 12 |** Structural and downstream sensitivity of the prespecified clinical domains.	P15
SI 13	**Supplementary Fig. 13 |** Additional evaluation of DynLifeNet and the validation-locked ensemble.	P16
SI 14	**Supplementary Fig. 14 |** Longitudinal multidomain remodeling instability and subsequent outcomes.	P17
SI Tables		
SI 15	**Supplementary Table 1 |** Cohort construction, baseline characteristics, and repeated-examination representativeness	P18

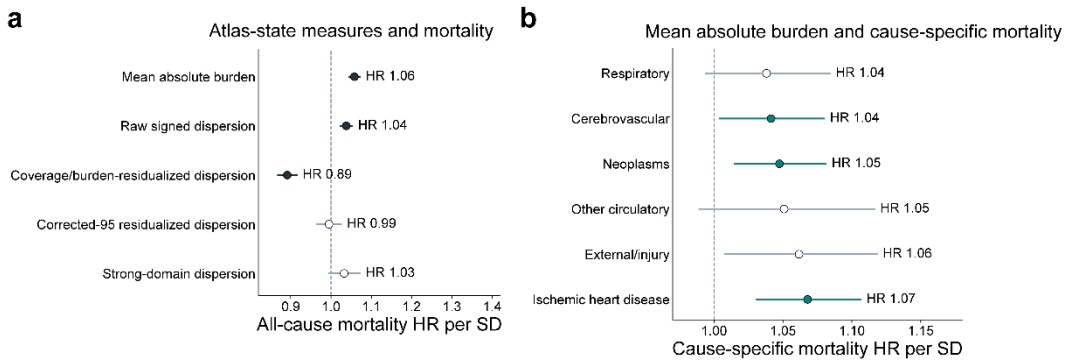
SI 16	**Supplementary Table 2 |** Atlas biomarker panel, harmonization summary, and local-code-derived abnormality coding	P20
SI 17	**Supplementary Table 3 |** Reference trajectories, same-age deviations, domain aggregation, and robustness analyses	P21
SI 18	**Supplementary Table 4 |** Detectable clinical phenotype shift windows and threshold sensitivity	P24
SI 19	**Supplementary Table 5 |** Clinical outcome associations, mortality diagnostics and disease-label face validity	P26
SI 20	**Supplementary Table 6 |** Age-banded domain co-deviation structure and network stability	P30
SI 21	**Supplementary Table 7 |** DynLifeNet endpoint support, prediction performance, leakage hardening and model reproducibility	P31
SI 22	**Supplementary Table 8 |** Multi-omics anchoring datasets, target mappings, negative controls and claim boundaries	P37



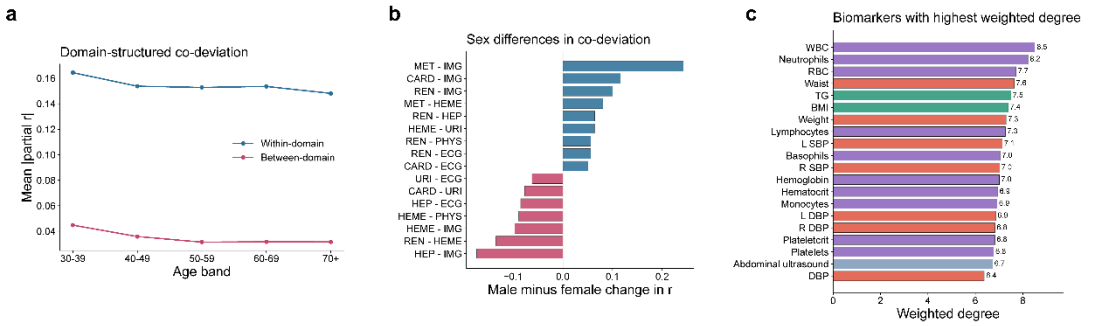
Supplementary Fig. 1 | Sex-specific age trajectories across the Health Atlas biomarker panel. Overview of age-associated trajectories for atlas biomarkers with sufficient age support for visualization. Each small panel shows the smoothed age-specific trajectory for a biomarker, stratified by sex. Pink and blue curves denote female and male trajectories, respectively, with shaded bands indicating 95% confidence intervals. Bottom histograms show the age distribution supporting each trajectory. Colored markers indicate the atlas module to which each biomarker belongs. Trajectories were estimated from the observed post-QC examination population and should be interpreted as empirical age patterns rather than disease-free normative references.



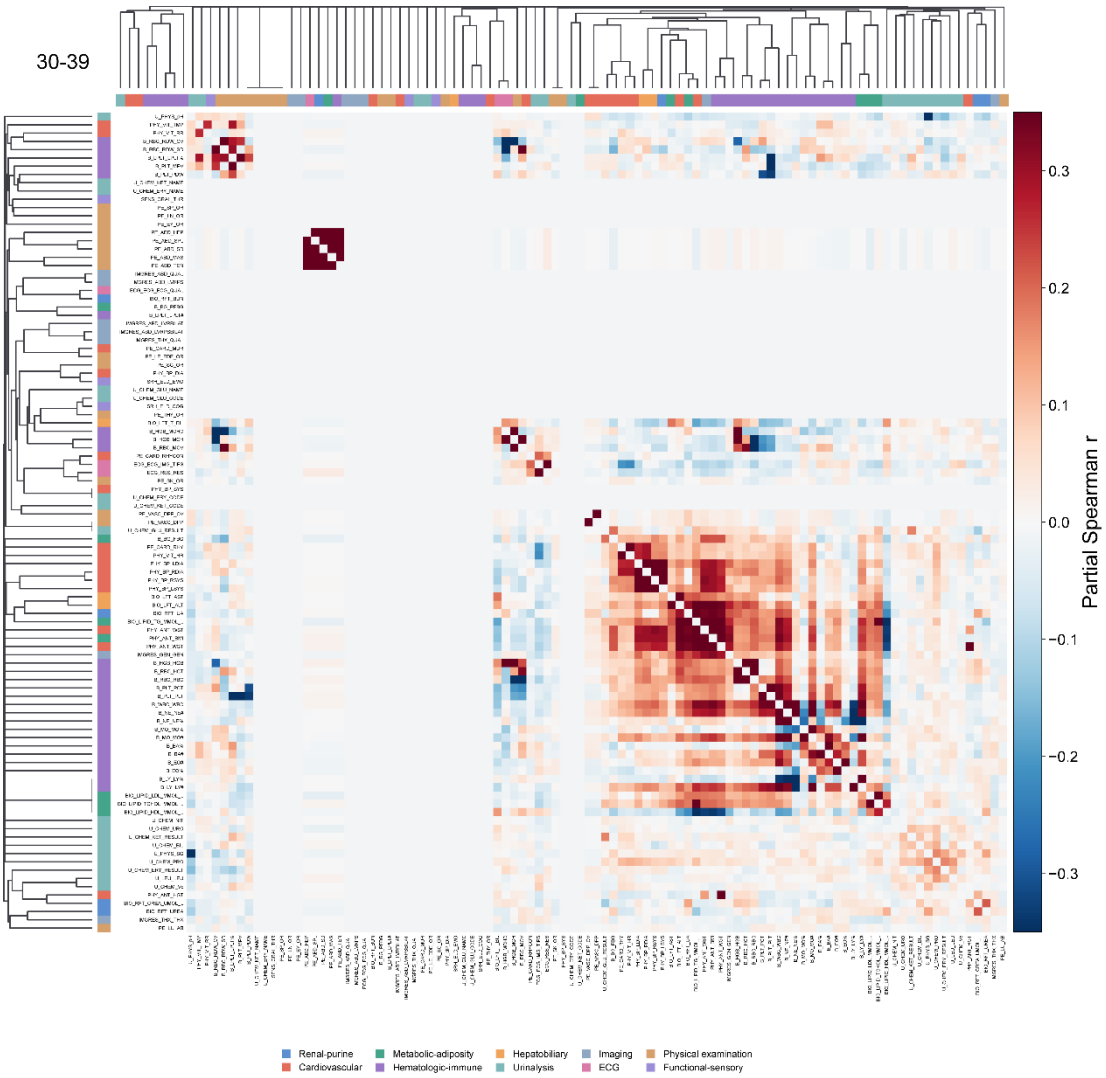
Supplementary Fig. 2 | Sensitivity analyses for detectable clinical phenotype shift windows. a, Threshold sensitivity of conservative detectable windows across 0.2, 0.3 and 0.5 SD cut-offs for each module-sex combination. Color indicates the age window in which the threshold was reached; NR denotes not reached within the evaluated age range. **b**, Evidence for sex-specific age-deviation shapes across modules, summarized as the sex-by-age interaction signal. Points compare analyses using all available visits and first-visit-only sensitivity analyses. **c,** First-visit sensitivity of point and conservative windows. Matched and changed indicators show whether the corresponding window remained unchanged when restricting to first visits. These analyses support the interpretation of detectable windows as threshold-defined clinical phenotype shifts rather than biological onset ages.



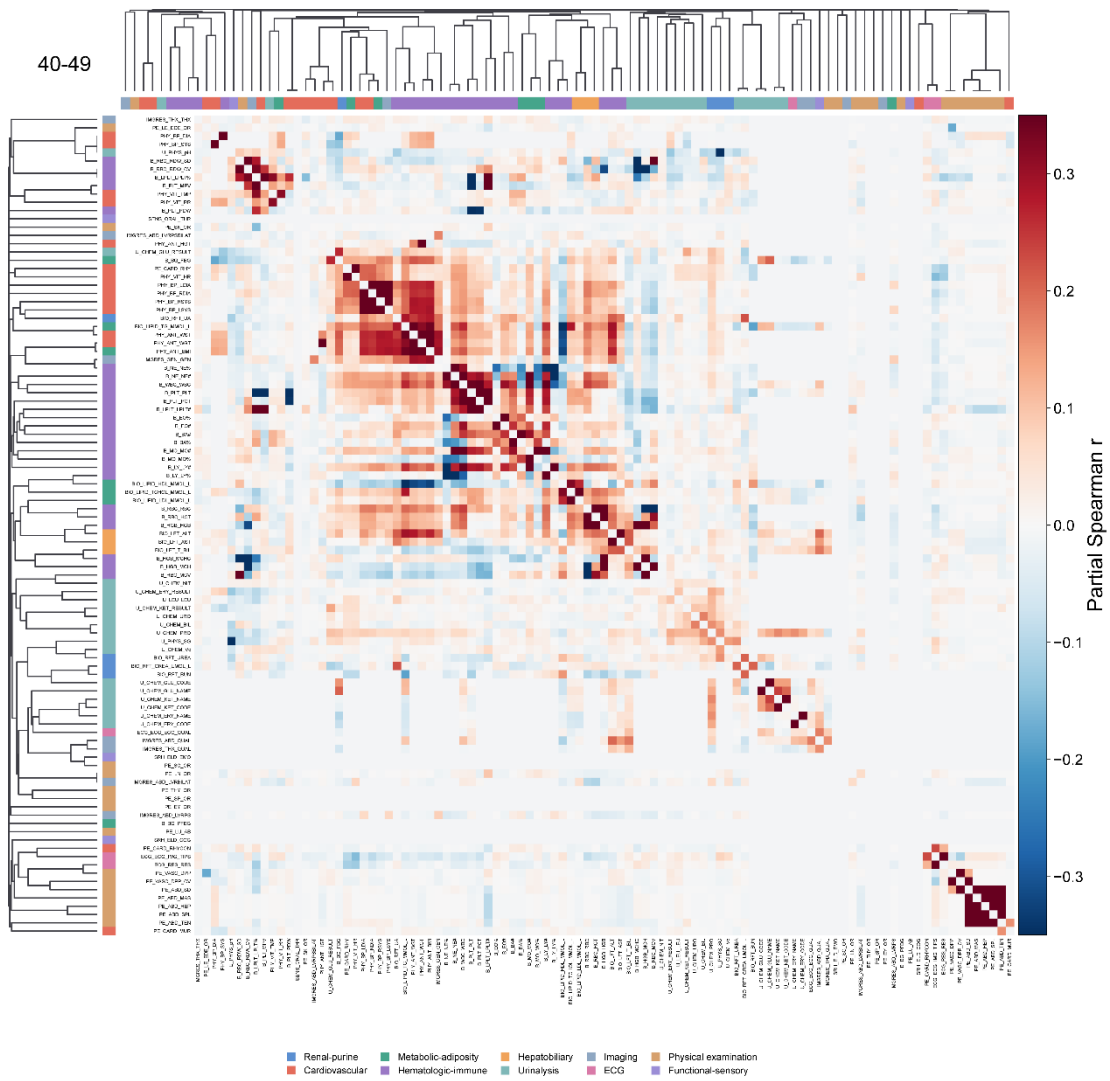
Supplementary Fig. 3 | Robustness of atlas-state mortality associations. a, All-cause mortality hazard ratios per SD for mean absolute burden, raw signed dispersion, coverage- and burden-residualized dispersion, corrected-95 residualized dispersion and dispersion across the three strongly reproduced domains. Models used the hardened common cohort and adjusted for disease burden, with sex-stratified baseline hazards. **b,** Cause-specific mortality hazard ratios per SD of mean absolute burden in the same hardened analysis framework. Filled points indicate FDR $q < 0.05$. The null corrected and strong-domain dispersion results do not support signed dispersion as an independently harmful asynchronous aging process.



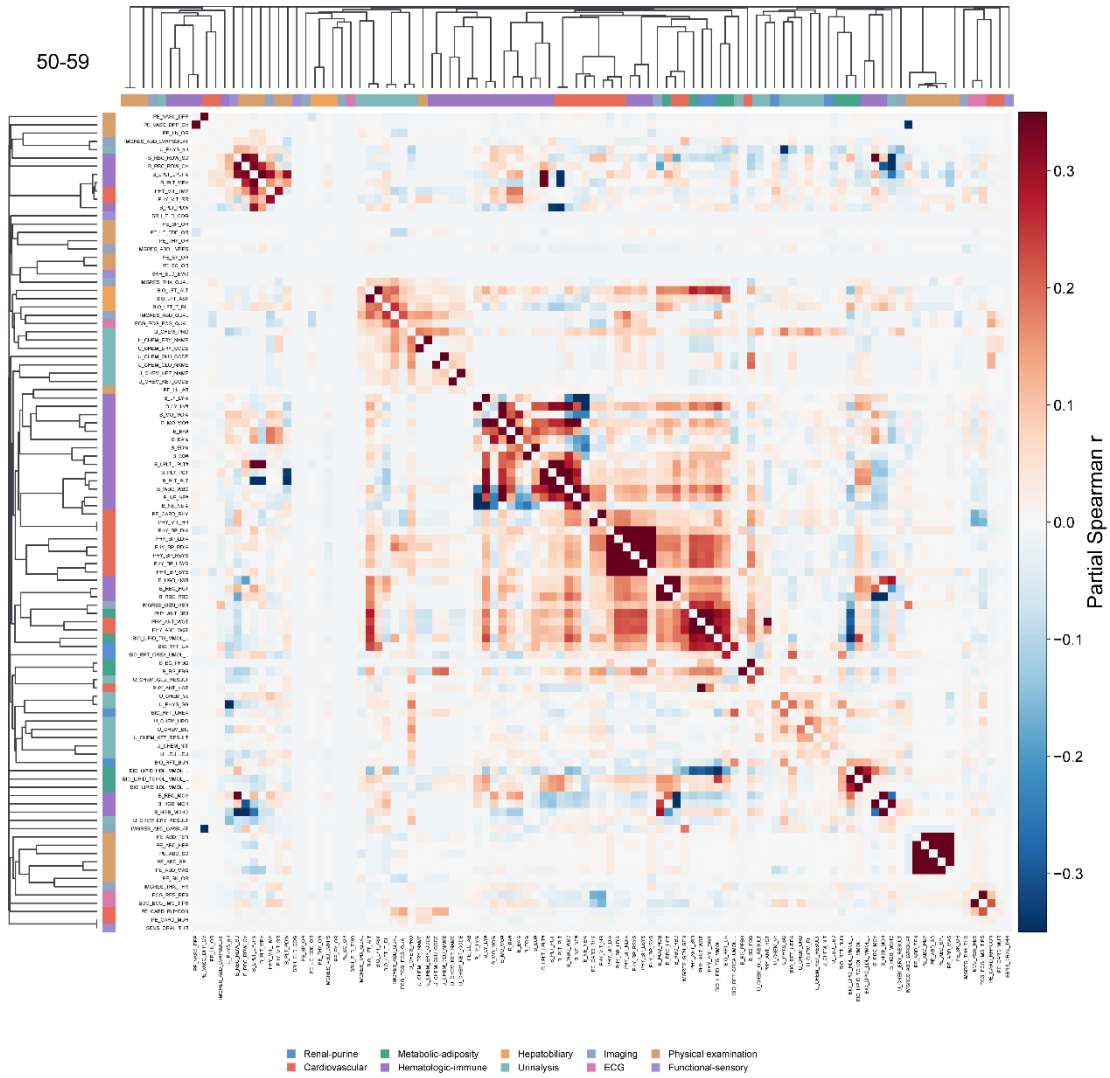
Supplementary Fig. 4 | Summary properties of age-banded domain and biomarker co-deviation. a, Mean absolute partial Spearman correlations within and between atlas domains across age bands, showing the separation between within-module and between-module co-deviation structure. **b,** Sex-specific network differences, shown as male-minus-female differences in module-pair correlations. Positive values indicate stronger correlations in males, whereas negative values indicate stronger correlations in females. **c,** Biomarkers with the highest weighted degree in the full co-deviation network. Bar colors indicate atlas domains. These network summaries describe age-banded co-deviation patterns and do not imply causal or directional interactions between physiological systems.



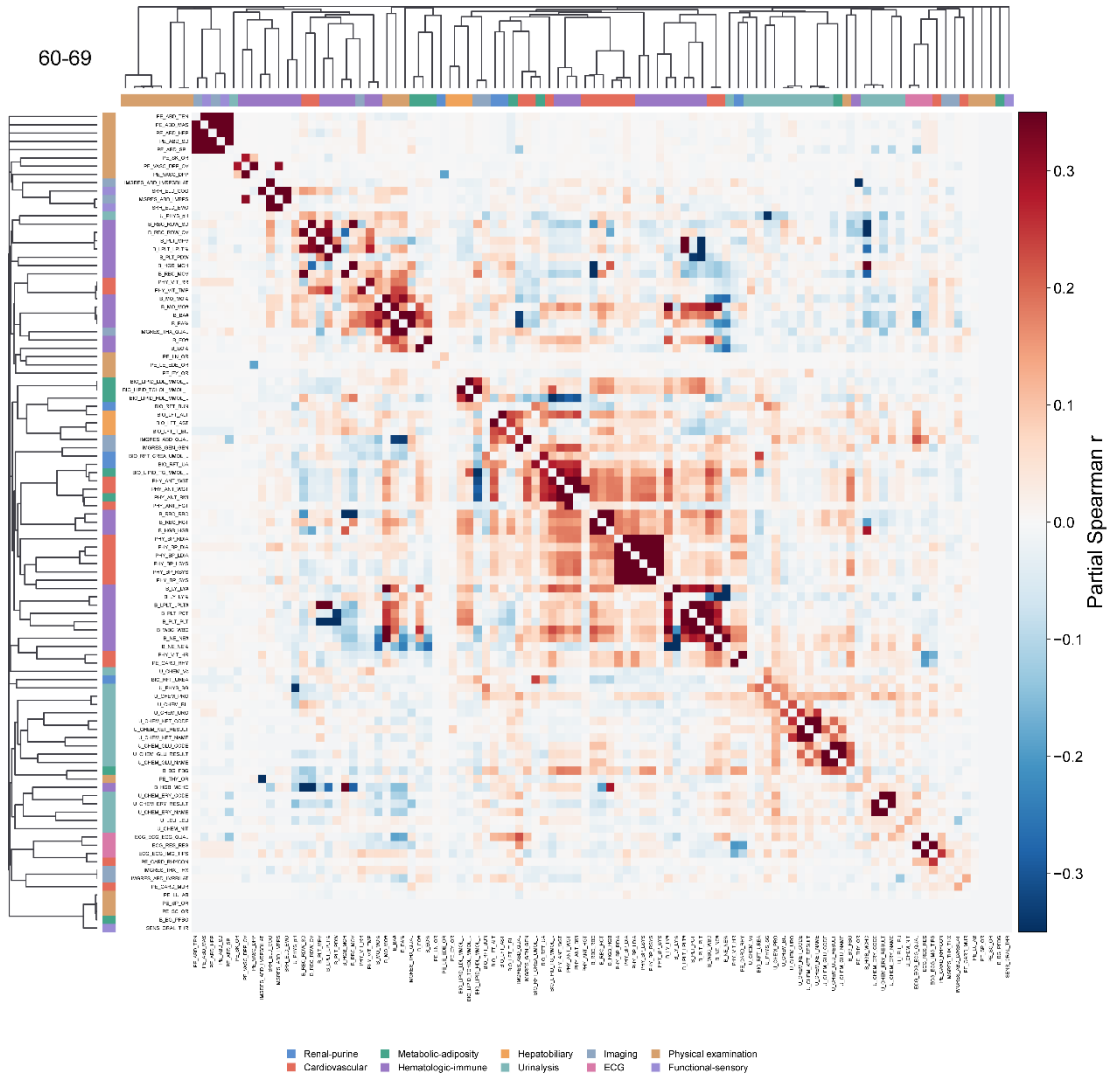
Supplementary Fig. 5 | Biomarker-level co-deviation structure in participants aged 30–39 years. Heatmap of age-banded biomarker co-deviation structure in the 30–39-year age group. Rows and columns represent atlas biomarkers, ordered by hierarchical clustering. The color scale shows partial Spearman correlation coefficients, with red indicating positive co-deviation and blue indicating negative co-deviation. Colored annotation bars indicate atlas domain membership. The matrix summarizes descriptive biomarker co-deviation within this age band and should not be interpreted as a causal network.



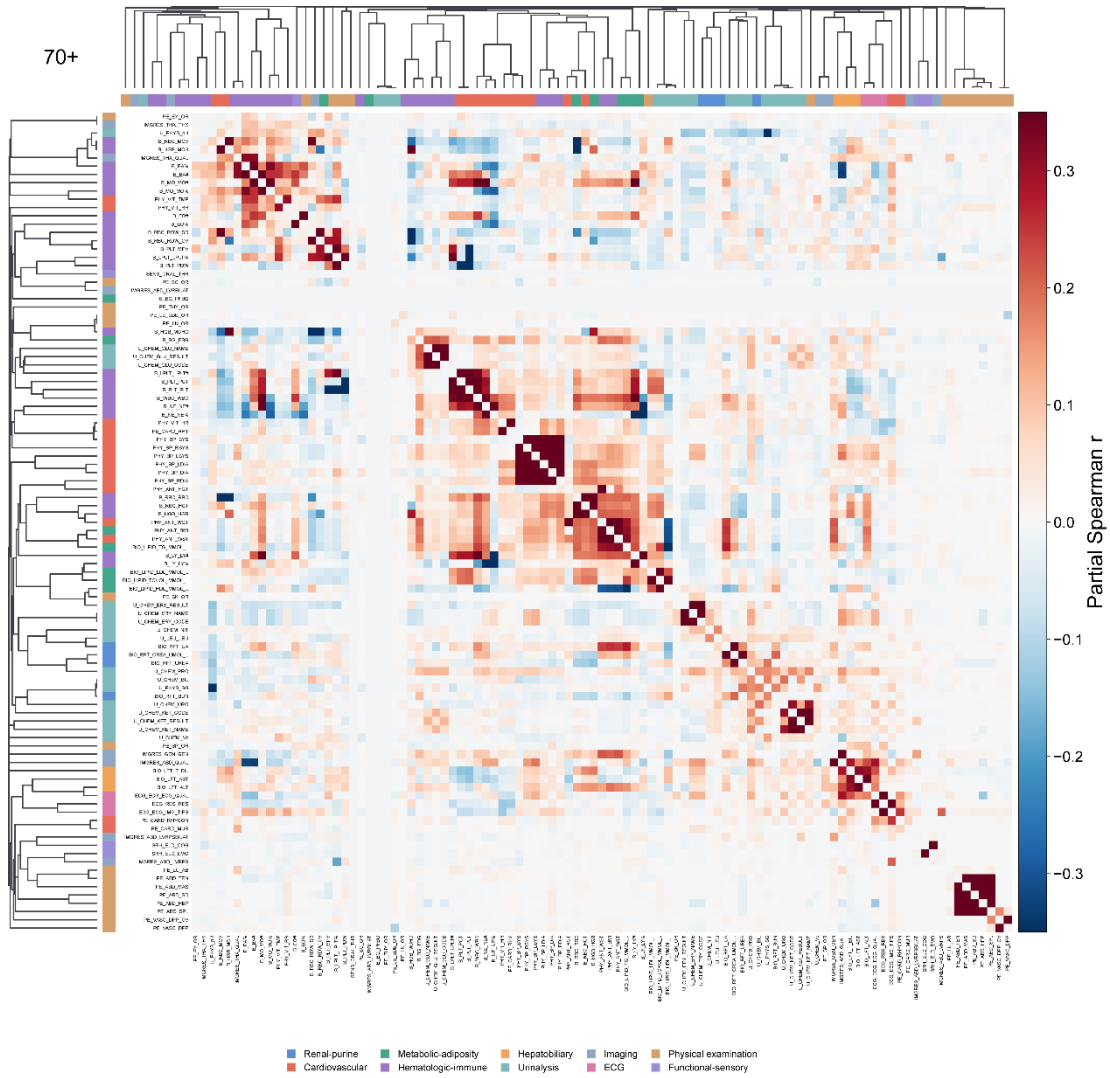
Supplementary Fig. 6 | Biomarker-level co-deviation structure in participants aged 40–49 years. Heatmap of age-banded biomarker co-deviation structure in the 40–49-year age group. Rows and columns represent atlas biomarkers, ordered by hierarchical clustering. The color scale shows partial Spearman correlation coefficients, with red indicating positive co-deviation and blue indicating negative co-deviation. Colored annotation bars indicate atlas domain membership. The matrix summarizes descriptive biomarker co-deviation within this age band and should not be interpreted as a causal network.



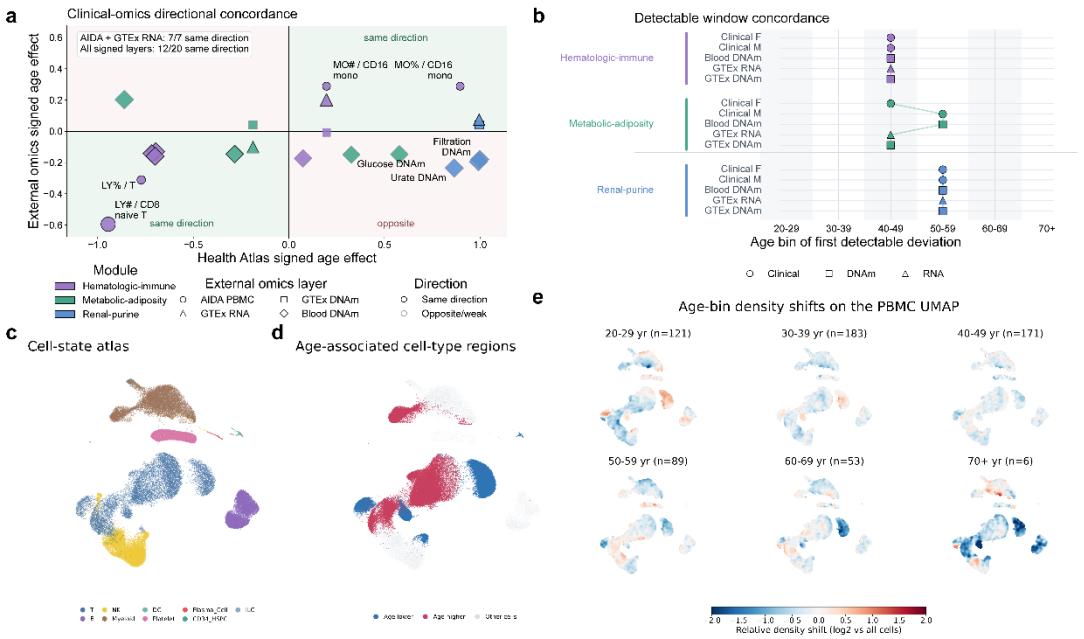
Supplementary Fig. 7 | Biomarker-level co-deviation structure in participants aged 50–59 years. Heatmap of age-banded biomarker co-deviation structure in the 50–59-year age group. Rows and columns represent atlas biomarkers, ordered by hierarchical clustering. The color scale shows partial Spearman correlation coefficients, with red indicating positive co-deviation and blue indicating negative co-deviation. Colored annotation bars indicate atlas domain membership. The matrix summarizes descriptive biomarker co-deviation within this age band and should not be interpreted as a causal network.



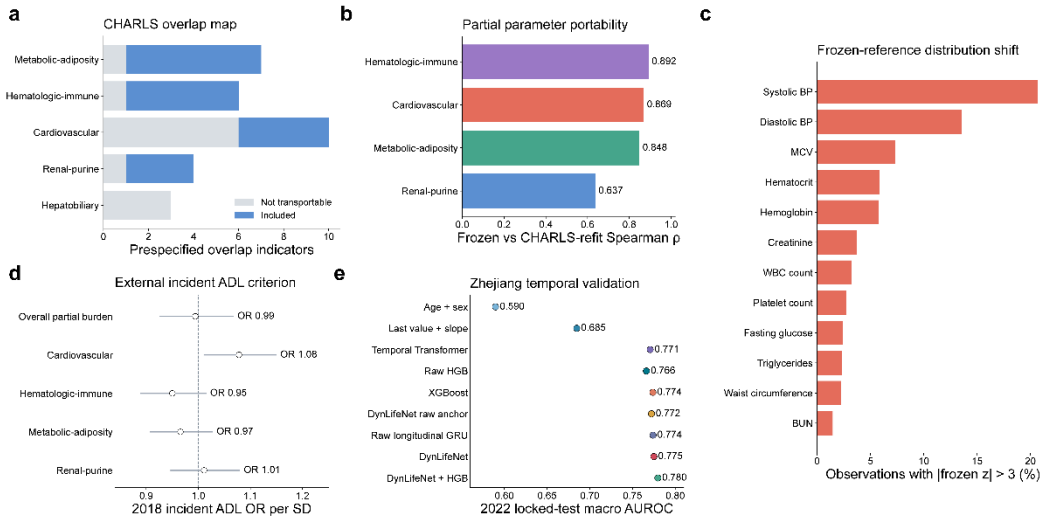
Supplementary Fig. 8 | Biomarker-level co-deviation structure in participants aged 60–69 years. Heatmap of age-banded biomarker co-deviation structure in the 60–69-year age group. Rows and columns represent atlas biomarkers, ordered by hierarchical clustering. The color scale shows partial Spearman correlation coefficients, with red indicating positive co-deviation and blue indicating negative co-deviation. Colored annotation bars indicate atlas domain membership. The matrix summarizes descriptive biomarker co-deviation within this age band and should not be interpreted as a causal network.



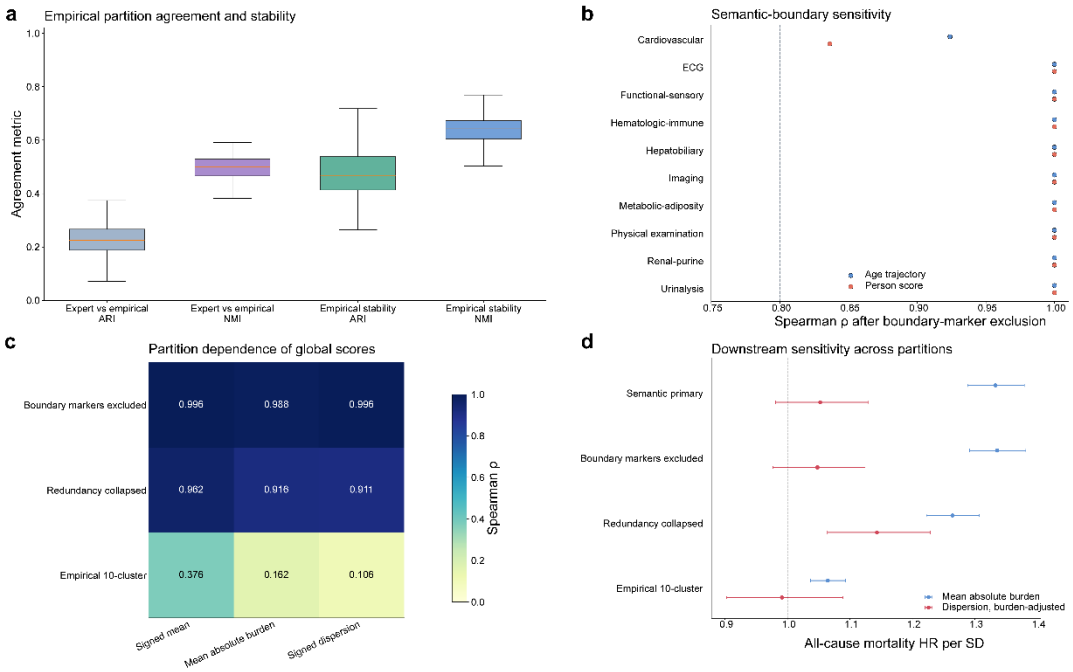
Supplementary Fig. 9 | Biomarker-level co-deviation structure in participants aged 70 years and older. Heatmap of age-banded biomarker co-deviation structure in the 70+ age group. Rows and columns represent atlas biomarkers, ordered by hierarchical clustering. The color scale shows partial Spearman correlation coefficients, with red indicating positive co-deviation and blue indicating negative co-deviation. Colored annotation bars indicate atlas domain membership. Because the 70+ bin combines a broader late-life age range, patterns in this panel should be interpreted cautiously in relation to nonlinearity, survivor selection and repeated-examination selection.



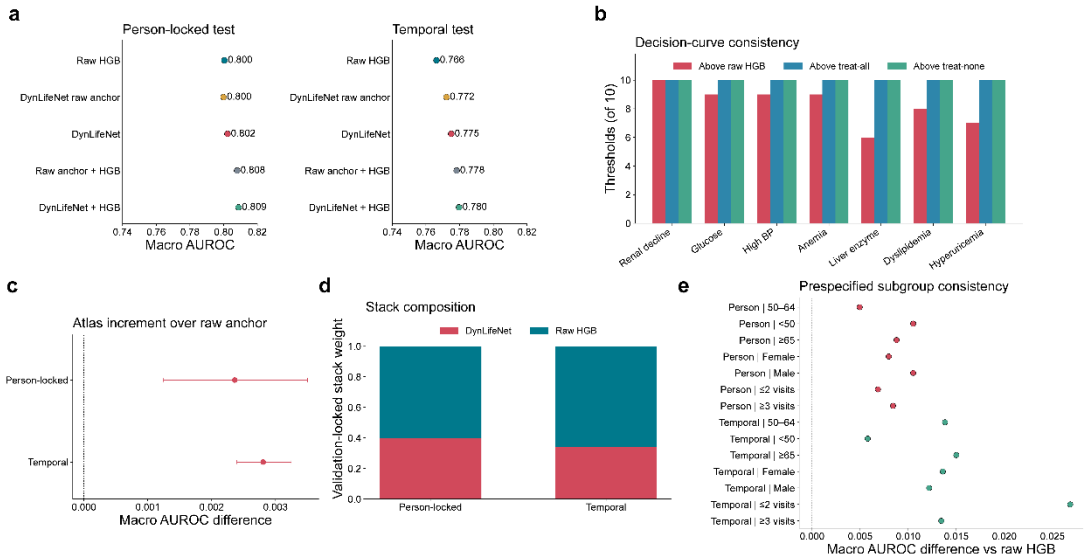
Supplementary Fig. 10 | Multi-omics anchoring of selected Health Atlas clinical axes. **a,** Directional concordance between atlas-derived signed age effects and external omics age effects across selected module-linked targets. Points are colored by atlas module and shaped by external evidence layer. The upper-right and lower-left quadrants indicate concordant directions between clinical atlas signals and external omics signals, whereas the off-diagonal quadrants indicate opposite directions. **b,** Concordance between detectable clinical phenotype shift windows and external omics age-associated signals across the hematologic-immune, metabolic-adiposity and renal-purine axes. Clinical, DNA methylation and transcriptomic evidence layers are shown on the same age-bin scale. **c,** Cell-state atlas projection from the external PBMC single-cell reference used for immune anchoring. **d,** Age-associated cell-type regions mapped onto the PBMC atlas. **e,** Age-bin density shifts on the PBMC UMAP, showing relative enrichment or depletion of cell-state regions across age groups. These analyses provide biological concordance and anchoring for atlas-derived aging axes, not mechanism validation or causal inference.



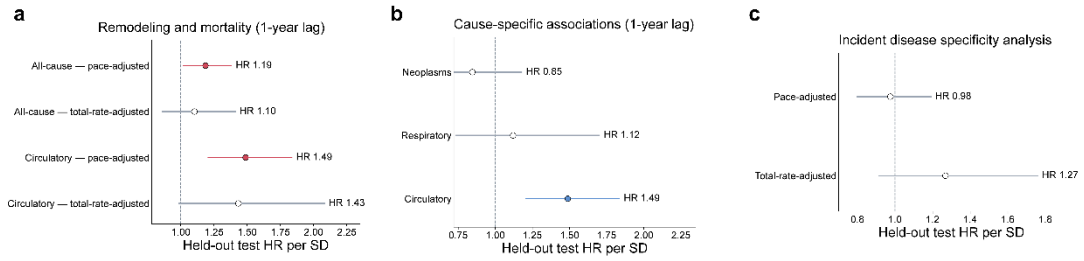
Supplementary Fig. 11 | Partial external transport and temporal validation of the Health Atlas framework. a, Prespecified overlap between Zhejiang core biomarkers and uniquely harmonized CHARLS indicators across four clinical domains. Grey segments denote nontransportable core indicators and blue segments denote included indicators. **b,** Spearman correlation between frozen Zhejiang domain scores and CHARLS-refitted scores. **c,** Distribution shift after applying frozen Zhejiang references to CHARLS; bars show the percentage of observations with |frozen z| > 3. **d,** Age- and sex-adjusted odds ratios per SD for 2018 incident activity-of-daily-living difficulty among CHARLS participants without difficulty in 2015. **e,** Macro AUROC in the Zhejiang earlier-year-to-later-year evaluation, including validation-tuned XGBoost and Temporal Transformer. Models were developed in 2016–2020, validated and calibrated in 2021, and evaluated in the locked 2022 test set.



Supplementary Fig. 12 | Structural and downstream sensitivity of the prespecified clinical domains. a, Agreement of empirical ten-cluster partitions with the clinical semantic assignments and bootstrap stability of the empirical partitions. Box plots summarize 200 outcome-blind resamples using adjusted Rand index and normalized mutual information. **b**, Spearman correlation of domain age trajectories and person scores after excluding high-ambiguity boundary biomarkers. **c**, Agreement of signed mean, mean absolute burden and signed dispersion between the primary semantic partition and boundary-excluded, redundancy-collapsed or empirical ten-cluster partitions. **d**, All-cause mortality hazard ratios per SD for mean absolute burden and burden-adjusted dispersion across alternative partitions. The results support the clinical domains as a stable semantic aggregation for most primary trajectories while showing that exact global scores and dispersion effects depend on partition choice.



Supplementary Fig. 13 | Additional evaluation of DynLifeNet and the validation-locked ensemble. a, Macro AUROC in the person-locked and Zhejiang temporal tests for raw HGB, DynLifeNet raw anchor, standalone DynLifeNet, raw anchor + HGB and DynLifeNet + HGB. **b**, Decision-curve consistency of DynLifeNet + HGB across endpoint-specific thresholds, compared with raw HGB, treat-all and treat-none strategies. **c**, Paired bootstrap macro-AUROC increment of standalone DynLifeNet over its matched raw anchor. **d**, Validation-locked ensemble weights for the person-locked and temporal protocols. **e**, Macro-AUROC differences between DynLifeNet + HGB and raw HGB across prespecified age, sex and visit-count subgroups. Subgroup results are consistency checks and are not powered interaction tests. Ensemble results are not evidence that the atlas branch alone outperforms raw HGB.



Supplementary Fig. 14 | Longitudinal multidomain remodeling instability and subsequent outcomes. a, Held-out mortality hazard ratios per SD of absolute residual remodeling after a one-year lag. Pace-adjusted and strict total-rate-adjusted models are shown for all-cause and circulatory mortality. **b**, Held-out cause-specific associations for neoplasm, respiratory and circulatory mortality. **c**, Negative specificity analysis for incident six-system clinical disease in the held-out test set. Points show hazard ratios and horizontal bars show 95% confidence intervals. These analyses support absolute remodeling instability as an exploratory prognostic state marker and do not establish harmful directional asynchrony or causality.

Supplementary Table 1 | Cohort construction, baseline characteristics, and repeated-examination representativeness

A. Cohort baseline

Metric	Source valid exam	Final atlas	Single visit	Repeated visit
Participants, n	345,539	189,095	31,600	157,495
Female, n (%)	177,039 (51.2%)	99,078 (52.4%)	13,008 (41.2%)	86,070 (54.6%)
Male, n (%)	168,500 (48.8%)	86,225 (45.6%)	15,942 (50.4%)	70,283 (44.6%)
Sex unavailable, n (%)	0 (0.0%)	3,792 (2.0%)	2,650 (8.4%)	1,142 (0.7%)
Age at first examination, median (IQR)	44.2 (33.5-54.6)	62.1 (54.5-70.0)	64.0 (52.3-77.8)	61.9 (54.7-69.2)
First examination year, median (IQR)	2010 (2008-2014)	2019 (2018-2020)	2018 (2016-2021)	2019 (2018-2020)
Visit count, median (IQR)	3 (1-14)	6 (2-10)	1 (1-1)	7 (4-10)
Follow-up years, median (IQR)	5.4 (0.0-13.5)	3.0 (0.1-4.9)	0.0 (0.0-0.0)	3.6 (1.3-5.0)
Final atlas biomarkers observed, median (IQR)		86 (53-90)	8 (7-12)	87 (81-90)
Final atlas clinical domains with any biomarker, median (IQR)		10 (9-10)	2 (2-4)	10 (9-10)

B. Frozen analysis cohort flow

Cohort stage	Participants	Deaths	Definition
Final atlas cohort	189,095	—	At least one retained atlas biomarker
First eligible atlas visit	158,901	—	At least five observed clinical domains
Positive-follow-up mortality cohort	153,024	4,830	Before model-specific complete-case restriction
Primary mortality model	147,492	4,599	Complete disease covariates

The 147,492 participants and 4,599 deaths define the primary disease-adjusted mortality base cohort.

C. Item flow and selection audit

Audit measure	Value
Reported items	860
Standardized items	402
Atlas biomarkers	99
Repeated-examination propensity AUC	0.993
Propensity >0.95	79.1%
Propensity <0.05	10.5%
Overlap-weight effective sample size	17,501
Maximum overlap-weighted |SMD|	0.010

AUC is in-sample discrimination for repeated versus single examination. SMD, standardized mean difference.

Supplementary Table 2 | Atlas biomarker panel, harmonization summary, and local-code-derived abnormality coding

Atlas component	Cont. n	Qual. indicator n	Total n	Records, n	Median participants per biomarker
Cardiovascular and vital signs	13	2	15	46,212,151	156,897
ECG	0	3	3	1,030,519	136,531
Functional-sensory	0	3	3	452,200	82,833
Hematologic-immune	25	0	25	10,268,218	132,429
Hepatobiliary	3	0	3	2,942,203	160,159
Imaging	0	7	7	1,746,939	54,194
Metabolic-adiposity	7	0	7	13,853,246	158,448
Physical examination	0	15	15	6,650,006	156,832
Renal-purine	4	0	4	2,558,935	123,400
Urinalysis	2	15	17	8,340,909	139,666
Total atlas panel	54	45	99	94,055,326	140,976
Qualitative raw-value mapping		45		105,091	

Supplementary Table 3 | Reference trajectories, domain aggregation, and robustness analyses

A. Atlas construction and primary definitions

Component	Parameter or check	Primary value or result
Reference trajectory	Age-sex-biomarker cell	Integer age-year × sex × biomarker
Reference trajectory	Age range	30–89 years
Reference trajectory	Minimum support	≥20 records per age-sex-biomarker cell; ≥100 records per age cell for domain-level summaries
Reference trajectory	Reference center	Smoothed age-sex median
Reference trajectory	Smoothing method	Centered 5-age-year rolling average, weighted by √n
Age-contrast trajectory	Reference window	30–39 years
Age-contrast trajectory	Continuous scale	Within-biomarker robust scale across the age curve
Age-contrast trajectory	Qualitative scale	0.10 absolute abnormality-rate difference
Same-age deviation	Continuous sigma	Smoothed IQR / 1.349, with smoothed SD fallback
Same-age deviation	z-score clipping	±5
Qualitative scaling	Binary-feature scale	Global exam-level abnormality rate p; $\sigma = \sqrt{[p(1-p)]}$
Qualitative scaling	Features requiring clipping	Rare or near-constant features: 21; positive-value clipped features: 31
Orientation	Numeric orientation	Empirical age-associated direction
Reference population	Primary reference population	Observed post-QC examination population
Reference sensitivity	Healthy-reference audit	20 matched comparisons; median Spearman r = 0.881
Reference sensitivity	Train-only reference audit	56 matched comparisons; median Spearman r = 0.913
Domain score	Primary domain score	Median of available oriented component scores within each domain and visit
Domain score	Standardization	Domain columns standardized across visits
Overall burden	Signed overall domain mean	Mean of observed signed standardized domain deviations

Component	Parameter or check	Primary value or result
Overall burden	Mean absolute domain burden	Mean absolute observed standardized domain deviation
Signed domain dispersion	Primary definition	SD of observed signed domain deviations
Domain aggregation sensitivity	Primary score versus alternative aggregations	Median Spearman r: equal mean = 0.949; coverage-weighted mean = 0.938; inverse-coverage-weighted mean = 0.927; PCA = 0.722
Burden/dispersion sensitivity	Alternative definitions	Median Spearman r: mean absolute domain burden = 0.782; signed domain dispersion SD = 0.772
Contribution sensitivity	Maximum top-marker contribution	Maximum absolute top-1 contribution share = 0.574

The ten domains are prespecified semantic clinical groupings.

B. Signed domain dispersion robustness

Analysis	Check	Value	Note
Residualization	Training sample	111,332	Training-only fit
Residualization	Covariates	Age splines, sex, year, domain count, domain count², mean absolute burden, signed mean	Applied unchanged outside training
Residualization	Raw dispersion R^2	0.958	95.8% explained after coverage and burden terms
Corrected-95 reconstruction	Analyzable biomarkers	95	Outcome-blind structural reconstruction
Corrected-95 reconstruction	Raw-dispersion agreement	Spearman ρ=0.396; n=158,901	Residualization-model R^2=0.856
Strong-domain sensitivity	Domains	ECG, functional-sensory, hepatobiliary	Raw-dispersion agreement ρ=0.065; n=153,966

The corrected-95 and strong-domain analyses are sensitivities; the residualization model was fitted in training data only.

C. Alternative-partition sensitivity

Alternative partition	Score n	Spearman ρ	Mortality n	Deaths	Burden-adjusted HR (95% CI)	P
High-ambiguity markers excluded	158,722	0.996	147,484	4,599	1.048 (0.977–1.124)	0.191
Redundancy-collapsed semantic	158,891	0.911	147,484	4,599	1.143 (1.064–1.228)	2.62e-04
Data-driven 10-cluster	143,264	0.106	141,032	4,550	0.991 (0.902–1.089)	0.851

HRs are per 1-SD dispersion and adjust for age, age², examination year, current and chronic disease burden, domain coverage, mean absolute burden, and signed mean.

D. Comparison with established or available constructs

Comparator	Paired n	Spearman ρ with signed dispersion	Scope
KDM acceleration	153,567	0.043	Training-derived adapted KDM
Homeostatic dysregulation	153,567	0.128	Young healthy training reference
Available multimorbidity count	150,090	-0.026	Available diagnoses only; not exhaustive

Correlations use the primary raw signed domain dispersion at the frozen first-eligible index.

Supplementary Table 4 | Detectable clinical phenotype shift windows and threshold sensitivity

Module	Sex	Point window at 0.3 SD	Conservative window at 0.3 SD	Threshold stability across 0.2–0.5 SD	n biomarkers at 0.3 SD	Bootstrap reached fraction	Any threshold involves 70+
Renal-purine	Female	50–59	50–59	Point stable; conservative variable	4	1.00	No
Renal-purine	Male	50–59	70+	Point variable; conservative stable	4	1.00	Yes
Cardiovascular/vital signs	Female	50–59	70+	Point stable; conservative variable	15	0.98	Yes
Cardiovascular/vital signs	Male	50–59	60–69	Both variable	15	1.00	Yes
Metabolic-adiposity	Female	40–49	50–59	Both stable	7	1.00	No
Metabolic-adiposity	Male	50–59	70+	Point stable; conservative variable	7	0.99	Yes
Hematologic-immune	Female	40–49	60–69	Point stable; conservative variable	25	1.00	No
Hematologic-immune	Male	50–59	50–59	Both variable	25	1.00	No
Hepatobiliary	Female	50–59	70+	Point variable; conservative stable	3	1.00	Yes
Hepatobiliary	Male	50–59	60–69	Both stable	3	1.00	No
Urinalysis	Female	50–59	70+	Both variable	17	0.99	Yes
Urinalysis	Male	60–69	Not reached	Both variable	17	0.97	Yes
Imaging	Female	50–59	Not reached	Both variable	7	0.96	Yes
Imaging	Male	70+	Not reached	Point variable; conservative stable not reached	7	0.70	Yes
ECG	Female	50–59	Not reached	Point variable; conservative stable not reached	3	0.97	No

Module	Sex	Point window at 0.3 SD	Conservative window at 0.3 SD	Threshold stability across 0.2–0.5 SD	n biomarkers at 0.3 SD	Bootstrap reached fraction	Any threshold involves 70+
ECG	Male	50–59	Not reached	Point variable; conservative stable not reached	3	0.97	No
Physical examination	Female	Not reached	Not reached	Both stable not reached	15	0.00	No
Physical examination	Male	Not reached	Not reached	Both stable not reached	15	0.00	No
Functional-sensory	Female	50–59	Not reached	Point variable; conservative stable not reached	3	0.63	No
Functional-sensory	Male	Not reached	Not reached	Both stable not reached	3	0.00	No

Across the 20 module-sex combinations, point windows were stable across the 0.2, 0.3 and 0.5 SD thresholds in 9 combinations, conservative windows were stable in 11 combinations, and at least one threshold-defined window involved the 70+ age bin in 9 combinations. “Not reached” indicates that the predefined deviation threshold was not reached within the evaluated age range. Stability includes stable non-reached results and therefore should not be interpreted as evidence for an early detectable shift. These windows are threshold-defined detectable clinical phenotype shift windows rather than biological onset ages.

Supplementary Table 5 | Clinical outcome associations, mortality diagnostics, and disease-label face validity

A. Frozen mortality cohorts and follow-up

Population	n	Deaths	Person-years	Median follow-up, years (IQR)
Positive-follow-up cohort	153,024	4,830	584,306.4	3.66 (3.04–4.67)
Primary disease-adjusted base cohort	147,492	4,599	—	Model-specific complete cases may be fewer

Administrative censoring date: 31 December 2023. The positive-follow-up cohort precedes model-specific complete-case restriction.

B. Global all-cause mortality associations

Exposure (per SD)	n	Deaths	HR (95% CI)	P	q	PH P
Mean absolute domain burden	147,492	4,599	1.058 (1.045–1.071)	3.91e-19	7.16e-19	2.16e-09
Raw signed domain dispersion	147,492	4,599	1.038 (1.024–1.052)	1.15e-07	1.58e-07	8.82e-06
Corrected-95 residualized dispersion	147,492	4,599	0.995 (0.966–1.025)	0.735	0.735	0.215
Strong-domain dispersion	143,840	4,414	1.033 (0.995–1.071)	0.089	0.098	0.507

Sex-stratified Cox models adjusted for age, age², examination year, current disease burden, and chronic disease burden. HRs are per 1-SD exposure.

C. Lag sensitivity

Exposure (per SD)	No lag	183-day lag	365-day lag
Mean absolute domain burden	1.058 (1.045–1.071)	1.055 (1.042–1.068)	1.047 (1.034–1.061)
Raw signed domain dispersion	1.038 (1.024–1.052)	1.035 (1.021–1.049)	1.029 (1.014–1.044)
Corrected-95 residualized dispersion	0.995 (0.966–1.025)	0.991 (0.962–1.021)	0.993 (0.963–1.024)
Strong-domain dispersion	1.033 (0.995–1.071)	1.031 (0.993–1.070)	1.024 (0.985–1.065)

The 183-day and 365-day analyses exclude deaths and follow-up within the specified lag.

D. Piecewise sensitivity for global exposures with PH signals

Exposure (per SD)	Deaths 0–730 d	HR 0–730 d	P	Deaths >730 d	HR >730 d	P
Raw signed domain dispersion	1,100	1.167 (1.137–1.198)	7.01e-31	3,499	1.015 (0.998–1.032)	0.079
Mean absolute domain burden	1,100	1.205 (1.177–1.233)	4.31e-56	3,499	1.030 (1.014–1.046)	1.42e-04

Piecewise split at 730 days; estimates address non-proportionality of the primary exposure term.

E. Cause-specific mortality for mean absolute domain burden

Cause of death	n	Deaths	HR (95% CI)	P	q
Respiratory	147,492	587	1.038 (0.994–1.084)	0.090	0.123
Cerebrovascular	147,492	779	1.041 (1.004–1.080)	0.028	0.039
Neoplasms	147,492	1,101	1.047 (1.015–1.081)	0.004	0.007
Other circulatory	147,492	247	1.051 (0.989–1.116)	0.107	0.147
External/injury	147,492	400	1.062 (1.008–1.118)	0.024	0.052
Ischemic heart disease	147,492	426	1.068 (1.031–1.106)	2.72e-04	4.27e-04

Non-target deaths were censored at death. Six causes correspond to Figure 3d.

F. First-eligible domain-specific all-cause mortality

Clinical domain (per SD)	n	Deaths	HR (95% CI)	P	q	PH P	PH q
Renal-purine	52,229	1,914	1.114 (1.074–1.156)	9.02e-09	4.51e-08	0.508	0.726
Cardiovascular	141,308	4,576	1.037 (1.013–1.062)	0.002	0.007	0.022	0.055

Clinical domain (per SD)	n	Deaths	HR (95% CI)	P	q	PH P	PH q
Metabolic-adiposity	54,763	2,202	1.038 (0.997–1.081)	0.073	0.122	0.006	0.032
Hematologic-immune	52,776	1,940	1.275 (1.222–1.331)	4.81e-29	4.81e-28	0.013	0.043
Hepatobiliary	54,967	2,185	0.946 (0.912–0.982)	0.003	0.008	2.76e-04	0.003
Urinalysis	145,369	4,370	1.021 (0.996–1.046)	0.104	0.148	0.802	0.983
Imaging	145,774	4,447	0.962 (0.935–0.991)	0.010	0.021	0.049	0.099
ECG	144,350	4,421	1.017 (0.987–1.047)	0.282	0.352	0.966	0.983
Physical examination	141,012	4,548	0.991 (0.966–1.016)	0.485	0.485	0.983	0.983
Functional-sensory	16,967	286	0.635 (0.223–1.806)	0.395	0.438	0.479	0.726

The base cohort contained 147,492 participants and 4,599 deaths; n and deaths shown here are actual domain-specific complete cases. q values use Benjamini–Hochberg correction.

G. Piecewise sensitivity for domains with PH q<0.05

Domain with PH signal	HR 0–730 d	q	HR >730 d	q
Metabolic-adiposity	1.086 (1.022–1.154)	0.012	0.995 (0.945–1.048)	0.861
Hematologic-immune	1.409 (1.323–1.501)	1.18e-25	1.170 (1.107–1.236)	6.74e-08
Hepatobiliary	0.911 (0.862–0.963)	0.002	1.030 (0.981–1.081)	0.278

Piecewise models used a common L2 penalizer of 0.001 and split follow-up at 730 days.

H. Disease-label face validity (unchanged)

Disease label	n	Cases	Measure	Value	Note
Cerebrovascular disease	167,276	1,327	Positive fraction	0.008	Same-visit label; healthy reference n = 77,788
Heart disease	167,263	1,818	Positive fraction	0.011	Same-visit label; healthy reference n = 77,788
Kidney disease	167,277	456	Positive fraction	0.003	Same-visit label; healthy reference n = 77,788
Eye disease	167,258	1,425	Positive fraction	0.009	Same-visit label; healthy reference n = 77,788
Nervous system disease	167,274	469	Positive fraction	0.003	Same-visit label; healthy reference n = 77,788
Other system disease	167,326	83,953	Positive fraction	0.502	Broad label category; same-visit label
Hypoglycemic reaction	20,856	671	Positive fraction	0.032	Same-visit label; healthy reference n = 77,788

Same-visit labels are descriptive face-validity checks and are not incident outcomes.

Supplementary Table 6 | Age-banded module co-deviation structure and network stability

A. Age-banded edge counts and stability

Age band	Raw edges with |r| ≥ 0.10	Adjusted edges with |r| ≥ 0.10	Bootstrap-stable adjusted edges	Repeat-sampling stable edges
30–39	4	4	4	7
40–49	7	3	3	9
50–59	6	4	3	6
60–69	7	3	3	6
70+	8	6	6	10
All age bands	32	20	19	38

B. Overall correlation and adjustment summary

Summary metric	Value	Interpretation
Tested module-pair-by-age combinations	225	45 module pairs × 5 age bands
Median absolute raw Spearman correlation	0.0416	Raw module co-deviation was modest
Median absolute adjusted partial Spearman correlation	0.0294	Adjustment attenuated the network signal
Same-sign fraction after adjustment	0.809	Most edges retained direction after adjustment
Bootstrap-stable adjusted edges	19	Stable edge instances across age bands
Repeat-sampling stable edges	38	Stable edge instances across 50 one-exam-per-person resampling runs

Adjusted partial correlations controlled for age within band, sex, calendar year and domain coverage. Edge counts refer to module-pair-by-age edge instances rather than causal or directional interactions. Repeat-sampling stability was evaluated across 50 one-exam-per-person resampling runs.

Supplementary Table 7 | DynLifeNet endpoint support, performance, frozen architecture, and diagnostics

A. Seven-endpoint support and definitions

Endpoint	Domain	Future abnormality	Baseline requirement	Test n	Events	Rate
Renal decline	Renal-purine	eGFR <60 or ≥20% decline	eGFR ≥60	9,881	906	9.2%
Glucose abnormality	Metabolic-adiposity	FBG ≥7.0 or postprandial glucose ≥11.1 mmol/L	Normal glucose	9,674	1,033	10.7%
High blood pressure	Cardiovascular	SBP ≥140 or DBP ≥90 mmHg	SBP <140 and DBP <90	4,931	2,803	56.8%
Anemia	Hematologic-immune	HGB <130 g/L (male) or <120 g/L (female)	Non-anemic	9,139	721	7.9%
Elevated liver enzymes	Hepatobiliary	ALT >40, AST >40, or GGT >60 U/L	No enzyme elevation	9,972	770	7.7%
Dyslipidemia	Metabolic-adiposity	Any TG, TC, LDL-C, or HDL-C threshold crossed	No dyslipidemia	4,849	1,324	27.3%
Hyperuricemia	Renal-purine	Uric acid ≥420 μmol/L (male) or ≥360 μmol/L (female)	No hyperuricemia	365	80	21.9%

All endpoints were evaluated 1–3 years after index; participants with the corresponding abnormality at baseline were excluded.

B1. Person-locked endpoint AUROC

Model	Renal decline	Glucose abnormality	High blood pressure	Anemia	Elevated liver enzymes	Dyslipidemia	Hyperuricemia	Macro AUROC
Last value + slope	0.759	0.930	0.762	0.829	0.726	0.738	0.790	0.791
Raw longitudinal GRU	0.769	0.939	0.771	0.838	0.744	0.740	0.735	0.791
Raw HGB	0.777	0.937	0.776	0.834	0.737	0.759	0.783	0.800
DynLifeNet raw anchor	0.779	0.940	0.776	0.841	0.742	0.756	0.764	0.800
DynLifeNet	0.782	0.941	0.780	0.842	0.742	0.759	0.770	0.802
DynLifeNet + HGB	0.788	0.942	0.784	0.844	0.747	0.768	0.789	0.809
Temporal Transformer	0.775	0.941	0.772	0.841	0.742	0.753	0.765	0.798
XGBoost	0.782	0.937	0.779	0.834	0.742	0.762	0.801	0.805

B2. Person-locked macro performance

Model	Endpoints	Macro AUROC	Macro PR-AUC	Macro Brier
Age + sex	7	0.607	0.259	0.131
Last-value logistic	7	0.786	0.458	0.109
Last value + slope	7	0.791	0.465	0.108
Raw longitudinal GRU	7	0.791	0.461	0.110
Raw HGB	7	0.800	0.481	0.107
DynLifeNet raw anchor	7	0.800	0.482	0.108
DynLifeNet	7	0.802	0.489	0.107
DynLifeNet + HGB	7	0.809	0.494	0.106
Temporal Transformer	7	0.798	0.478	0.108
XGBoost	7	0.805	0.491	0.106

Brier scores are lower when better. DynLifeNet is the canonical atlas-residual model; DynLifeNet + HGB is a validation-locked post-training ensemble.

C. Zhejiang earlier-year-to-later-year performance

Model	Endpoints	Macro AUROC	Macro PR-AUC	Macro Brier
Age + sex	6	0.590	0.204	0.121
Last value + slope	6	0.685	0.289	0.153
Raw longitudinal GRU	6	0.774	0.392	0.114
Raw HGB	6	0.766	0.379	0.114
DynLifeNet raw anchor	6	0.772	0.384	0.115
DynLifeNet	6	0.775	0.386	0.115
DynLifeNet + HGB	6	0.780	0.393	0.113
Temporal Transformer	6	0.771	0.385	0.113
XGBoost	6	0.774	0.388	0.114

D. Frozen architecture, two-stage training, and hyperparameters

Block	Parameter	Value	Role
identity	model name	DynLifeNet	Canonical publication name
architecture	overall design	raw-anchored atlas residual	Endpoint-specific future abnormality prediction
raw branch	visit encoder	missingness-aware projection + GRU + masked attention pooling	Encodes repeated raw biomarker visits
summary branch	subject summary	latest values + within-person slopes + observation counts + age + sex	Encodes compact longitudinal summaries
atlas branch	token encoder	value features + biomarker embedding + clinical-domain embedding	Encodes observed biomarker tokens
atlas branch	within-visit aggregation	endpoint-specific masked attention	Creates an endpoint-conditioned visit vector
atlas branch	temporal encoder	structured GRU + masked attention pooling	Creates an endpoint-specific atlas state
combination	final logit	raw anchor logit + safety gate × bounded atlas residual	Preserves the raw anchor while allowing bounded atlas correction
initialization	atlas residual output	zero	Starts with no atlas correction
initialization	safety gate bias	-2	Starts with a small residual contribution
training	stage 1	train raw and summary anchor components	Class-weighted binary cross-entropy with raw and summary auxiliary losses
training	stage 2	freeze anchor and train atlas residual components	Final binary cross-entropy plus structured auxiliary and residual regularization
training	optimizer	AdamW	Used in both training stages
training	learning rate / weight decay	0.0007 / 0.0002	Used in both training stages
training	batch size	512	Participants per batch
training	maximum epochs, anchor / atlas	9 / 18	Maximum before early stopping
training	early-stopping patience	4 epochs	Validation macro AUROC

Block	Parameter	Value	Role
training	gradient clip norm	5.0	Applied in both training stages
loss	raw / summary auxiliary weights	0.1 / 0.1	Anchor stage
loss	structured auxiliary weight	0.1	Atlas stage
loss	residual L2 weight	0.001	Atlas stage
configuration	hidden dimension	48	Validation-selected frozen setting
configuration	dropout	0.12	Validation-selected frozen setting
configuration	positive-class weight cap	20.0	Validation-selected frozen setting
reproducibility	training seeds	20260731, 20260817, 20260903	Three-seed selected configuration
confirmation	evaluation protocols	person-locked test; Zhejiang earlier-year-to-later-year test	Test outcomes were not used for model selection

E1. Paired bootstrap comparisons

Protocol	Comparison	Δ macro AUROC (95% CI)	P value	BH q value
Person-locked	DynLifeNet vs DynLifeNet raw anchor	0.0024 (0.0012–0.0035)	0.002	0.003
Person-locked	DynLifeNet + HGB vs Raw HGB	0.0083 (0.0041–0.0127)	0.002	0.003
Person-locked	DynLifeNet + HGB vs Raw anchor + HGB	0.0008 (0.0002–0.0014)	0.012	0.012
Zhejiang temporal	DynLifeNet vs DynLifeNet raw anchor	0.0028 (0.0024–0.0032)	0.002	0.002
Zhejiang temporal	DynLifeNet + HGB vs Raw HGB	0.0134 (0.0119–0.0148)	0.002	0.002
Zhejiang temporal	DynLifeNet + HGB vs Raw anchor + HGB	0.0014 (0.0012–0.0017)	0.002	0.002

Each comparison used 1,000 paired bootstrap replicates.

E2. Additional algorithm benchmark comparisons

Protocol	Comparison	Δ macro AUROC (95% CI)	P	BH q
Participant-locked	DynLifeNet vs XGBoost	−0.0029 (−0.0110–0.0045)	0.430	0.430
Participant-locked	DynLifeNet vs Temporal Transformer	0.0040 (−0.0002–0.0084)	0.068	0.136
Zhejiang temporal	DynLifeNet vs XGBoost	0.0011 (−0.0012–0.0034)	0.342	0.342
Zhejiang temporal	DynLifeNet vs Temporal Transformer	0.0043 (0.0027–0.0059)	0.002	0.004

Benjamini–Hochberg correction was applied to the two additional algorithm comparisons within each evaluation protocol.

E2. Calibration

Protocol	Model	Macro Brier	Median calibration slope
Person-locked	Raw HGB	0.107	0.979
Person-locked	DynLifeNet raw anchor	0.108	1.003
Person-locked	DynLifeNet	0.107	0.979
Person-locked	DynLifeNet + HGB	0.106	1.197
Zhejiang temporal	Raw HGB	0.114	1.002
Zhejiang temporal	DynLifeNet raw anchor	0.115	0.942
Zhejiang temporal	DynLifeNet	0.115	0.881
Zhejiang temporal	DynLifeNet + HGB	0.113	1.113

Brier scores and calibration slopes are locked-test evaluations; calibration choices were selected using validation data.

E3. Decision-curve summary

Protocol	Comparison	Above comparator	Above treat-all	Above treat-none	Mean Δ net benefit
Zhejiang temporal	DynLifeNet vs Raw HGB	26/60	59/60	38/60	-0.0011
Zhejiang temporal	DynLifeNet + HGB vs Raw HGB	49/60	59/60	40/60	0.0014
Zhejiang temporal	DynLifeNet + HGB vs Raw anchor + HGB	38/60	59/60	40/60	0.0000
Person-locked	DynLifeNet vs Raw HGB	34/70	70/70	67/70	0.0000
Person-locked	DynLifeNet + HGB vs Raw HGB	58/70	70/70	70/70	0.0020
Person-locked	DynLifeNet + HGB vs Raw anchor + HGB	42/70	70/70	70/70	0.0004

Counts pool the prespecified threshold grid across endpoints; net-benefit deltas are averaged across endpoints.

E4. Subgroup summary

Protocol	Comparison	Positive Δ strata	Δ macro AUROC range
Zhejiang temporal	DynLifeNet vs DynLifeNet raw anchor	6/7	-0.0005 to 0.0034
Zhejiang temporal	DynLifeNet vs Raw HGB	6/7	-0.0067 to 0.0258
Zhejiang temporal	DynLifeNet + HGB vs Raw HGB	7/7	0.0058 to 0.0268
Person-locked	DynLifeNet vs DynLifeNet raw anchor	7/7	0.0000 to 0.0031
Person-locked	DynLifeNet vs Raw HGB	4/7	-0.0132 to 0.0051
Person-locked	DynLifeNet + HGB vs Raw HGB	7/7	0.0049 to 0.0105

E5. Continuous net reclassification improvement

Evaluation set	Comparison	Macro continuous NRI (95% CI)	Event component	Nonevent component
Person-locked	DynLifeNet vs DynLifeNet raw anchor	0.2102 (0.1677–0.2520)	0.1665	0.0437
Person-locked	DynLifeNet + HGB vs Raw HGB	0.3445 (0.3031–0.3866)	0.0959	0.2486
Person-locked	DynLifeNet + HGB vs Raw anchor + HGB	0.1497 (0.1132–0.1890)	0.0852	0.0645

Supplementary Table 8 | Multi-omics anchoring datasets, target mappings, negative controls and claim boundaries

A. Atlas axis-to-target mapping summary

Atlas axis	Atlas biomarkers	Target genes and biomarker-gene links	CpG links	Blood DNAm age signal	Interpretation boundary
Hematologic-immune	25	61 target genes; 236 biomarker-gene links	1,000	FDR < 0.05 fraction = 0.731	Curated anchoring; not a causal map
Metabolic-adiposity	7	40 target genes; 55 biomarker-gene links	1,415	FDR < 0.05 fraction = 0.747	Curated anchoring; not a causal map
Renal-purine	4	23 target genes; 33 biomarker-gene links	1,275	FDR < 0.05 fraction = 0.754	Curated anchoring; not a causal map

B. External omics evidence layers and interpretation limits

Evidence layer	Data source	Data scale	Features or tests	Age support	Use and claim boundary
PBMC single-cell composition	AIDA PBMC single-cell atlas	625 donors; 1,265,624 donor-profiled cells	97 cell types	19.0–77.0 years	Immune-composition concordance; no multivariable audit; not causal immune remodeling
Bulk transcriptome	GTEx v8 bulk RNA	Per tissue/context n = 85–803; median n = 258	124 target genes; 6,125 gene-tissue-module tests	24.5–74.5 years	Cross-tissue target-gene age concordance; technical and cell-composition covariates not fully modeled; not direct regulation or causality
Tissue DNA methylation	GTEx DNAm, GSE213478	Per tissue/context n = 47–224; median n = 54	3,348 CpGs; 30,141 CpG-tissue-module tests	24.5–74.5 years	Methylation-linked genomic bridge; technical and cell-composition covariates not fully modeled; not proof of gene regulation
Whole-blood DNA methylation	GSE87571	729 age-tested samples; 732 metadata rows	2,122 CpGs; 2,122 target CpG rows	14.0–94.0 years	Blood DNAm age concordance near target genes; sex, batch and blood-cell composition not fully adjusted; not direct mechanism validation

Evidence layer	Data source	Data scale	Features or tests	Age support	Use and claim boundary
Kidney-localization evidence	KPMP and GSE183279 kidney spatial transcriptomics	38 matrices; 1,266,971 cells/spots	23 renal-purine target genes summarized	Not available in local processed table	Kidney-context plausibility; no age or covariate model; not causal renal-pathway validation
Kidney-function methylation bridge	Kidney-function EWAS supplement overlap	4 renal bridge genes; 6 CpG IDs	ANKRD11, PHB2, PTPN6, TNRC18	Not available in local overlap table	Indirect renal-function methylation bridge; source EWAS not re-modeled; not a direct urate-transport causal test
Adipose single-nucleus evidence	GSE235529 adipose snRNA-seq	20 donors; 10 older and 10 younger	5 metabolic signatures; 5 old-versus-young contrasts	Young versus old groups; exact ages not retained locally	Adipose-cell context for metabolic-adiposity targets; no multivariable audit; plausibility only
Negative-control audit	Target-universe permutation controls	177 modality–axis–context tests	1,000 permutations per context	Not applicable	Median empirical $P = 0.554$; empirical $P < 0.05$ in 19/177 tests; bias audit only, not genome-wide enrichment.

Full biomarker-to-gene and biomarker-to-CpG mappings are provided in Supplementary Data 1. Dataset scale, negative-control audits and interpretation boundaries are summarized here.